3 Functional role of scaffolds with different geometries as a template for physiological callus formation: evaluation of collagen 3D assembly[1]

3.1 Abstract

Bone tissue regeneration involves different healing stages and the resulting final hard tissue is formed from natural templates such as fibrous collagen, soft and hard callus and capillary bed. This work aims to evaluate the efficiency of different scaffold geometries with a novel approach: exploring the relationships among scaffold morphologies, cell activity and collagen 3D organization, which serves as a natural template for subsequent mineralization. Among the possible systems to fabricate scaffolds, solvent casting with particulate leaching and microfabrication were used to produce random versus ordered structures from poly-d,l-lactic acid. In vitro biological testing was carried out by culturing a human osteosarcoma derived osteoblast cell line (MG63) and measuring material cytotoxicity, cell proliferation and migration. Assemblage of collagen fibers was evaluated. A preliminary study of collagen distribution over the two different matrices was performed by confocal laser microscopy after Direct Red 80 staining. Both of the scaffolds were seen to be a good substrate for cell attachment, growth and proliferation. However, it seems that

[1]The work presented in this chapter was published in Journal of Tissue Engineering and Regenerative Medicine as Stoppato M, et al., Functional role of scaffold geometries as a template for physiological ECM formation: evaluation of collagen 3D assembly. Journal of Tissue Engineering and Regenerative Medicine (2013), 7(2), 161–8.

random, rather than regular, well-ordered porosity, induces a more proper collagen fiber distribution and organization, similar to the natural one formed in the early stages of bone repair.

3.2 Introduction

Bone fracture healing can be considered as a four-step process. The initial inflammatory cellular response due to a fracture leads to the formation of soft callus (fibrocartilage), serving as a guide for the subsequent hard callus production, i.e., the first osteogenetic phase[62, 1]. Cortical and trabecular bone are developed and remodeled in the final stage. Each newly-formed tissue starts to grow from the previous tissue, which represents the appropriate template. The whole mechanism of bone healing comprises these overlapping stages [64, 65, 66].

The repair process involves different cells and molecules which contribute at different levels, playing precise biological roles. These include inflammatory cells, vascular cells, osteoblasts, osteoclasts, pro-inflammatory cytokines, pro-osteogenic factors and angiogenic factors [133].

Collagen represents the most important and the richest protein of connective tissue in mammals and it is the main constituent of extracellular matrix (ECM) and soft callus. It is a fibrous protein and several different types have been identified. Collagen type I is predominant in developing bone tissue and it is principally produced by osteoblasts.

The main focus of bone tissue engineering is to support and guide the healing process and bone reconstruction, in our case, by using scaffolds designed as temporary ECMs able to direct normal cell function [3, 134]. Recent studies have shown that cells are sensitive to chemistry, stiffness and surface properties of the scaffold [3, 92, 135]. Therefore, successful bone repair depends on the three-dimensional (3D) scaffold design which works as a bioactive support for host cells as they are organized into a functional tissue [136, 137]. Important matrix parameters are pore size, distribution and interconnectivity, mechanical integrity and surface characteristics [41, 75, 138, 139, 140, 141].

In recent years, extensive interest has been focused on the relationship between scaffold morphology and cell response, in terms of proliferation and differentiation. Bone tissue regeneration has been addressed to use scaffolds with a specific morphology, pore size and interconnectivity to enhance cell penetration, appropriate nutrient supply, waste removal and neoangiogenesis [142, 143]. Furthermore, in a previous study [144] microfabricated scaffolds with two different pore size were compared and osteoblasts penetration and migration inside the two structures was studied.

The work presented here falls within the first stage of bone formation and aims

to evaluate how different scaffold morphologies influence osteoblast activity as well as collagen assembly. Collagen organization and callus formation play fundamental roles as gap filler and blueprint for subsequent ECM maturation and mineralization [145]. The ECM of cancellous bone is characterized by irregularly arranged collagen fibers and prior callus formation is fundamental for angiogenesis and final tissue formation [146]. Identifying the geometric structure of matrix (pore size and shape) and its role in collagen fiber organization represents a good starting point to address a strategy for directing a more biomimetic and controlled mineralization [3].

In this work poly-d,l-lactic acid (PdlLA) was used. This polymer is widely employed in scaffold production for bone tissue regeneration due to its mechanical properties and processability into a variety of shapes and sizes [123, 147, 148, 149, 150].

Two different models of scaffolds were produced: ordered, structured microfabricated scaffolds with a spatially well defined porosity and salt-leached sponges with interconnected, randomly distributed pores.

Human osteosarcoma derived osteoblasts (cell line MG63) were used for preliminary in vitro biological evaluations. The non-cytotoxicity of the processed material was confirmed by LDH in vitro assay while cell proliferation was evaluated by alamarBlue assay. Cell growth and distribution as well as morphological evaluations were assessed by confocal laser microscopy (CLM) imaging after cell staining with Rhodamine Phalloidine and DAPI. Scanning electron microscopy (SEM) imaging further confirmed images obtained through CLM analysis [151]. Collagen production and organization were analyzed using CLM after Direct Red 80 staining [152, 153, 154, 155].

3.3 Materials and Methods

Materials

Poly-d,l-lactic acid (PdlLA, type RESOMER® 207, MW= 252 kDa) was purchased from Boehringer Ingelheim, Germany (polymer was used without further purification) and dichloromethane (DCM) and dimethylformamide (DMF) were purchased from BDH Chemicals (UK) and J.T.Baker (Holland), respectively.

Scaffolds

Scaffolds with regular geometry were produced with a home-made microfabrication apparatus [144]. PdlLA was dissolved in dichloromethane: dimethylformamide (70:30 v/v) to prepare a 20% (w/v) solution. This concentration was selected as being the optimal one after performing multiple microfabrication tests. Scaffolds were made with equidistant rows on 20 sequential orthogonal layers produced by extrusion of solution filaments through a syringe needle (33 gauge). The distance between rows was set to 375 µm.

Sponges with randomly distributed pores were produced by solvent casting into cylinders and particulate leaching [156, 157, 158]. PdlLA was dissolved in dichloromethane: dimethylformamide (70:30 v/v) to prepare a 6.5% (w/v) solution. Sieved NaCl particulates with a dimensional range between 240 and 315 µm were mixed in, obtaining a final concentration polymer/porogen of 1:40 w/w. The mixture was air dried (24-36 hours) and immersed in deionized water (dH2O) for 3 days with change every 6 hours for the removal of the porogen.

All the scaffolds, which were prepared by casting into cylinders were cut into discs with a diameter of 10 mm sterilized with aqueous ethanol solution 70% (v/v) at 4°C for 24 hours and dried under a hood at room temperature.

Scaffold characterization

Scanning Electron Microscopy (SEM) imaging

Scanning electron microscopy (Supra 40 Zeiss, operating mode: high vacuum, secondary electron detector) was used for the observation of scaffold morphologies. The

samples were sputter-coated with a thin gold layer under argon atmosphere (SEM Coating Unit PS3, Assing S.p.A., Rome, Italy).

Scaffold porosity evaluation

Considering the different geometrical features of scaffolds, two different methods were chosen to calculate scaffold porosity. Microfabricated scaffold porosity was evaluated from SEM images by ImageJ software [159, 160] while salt leached scaffold porosity by a liquid displacement method similar to a previously described technique [161, 162, 163].

Microfabricated scaffold pore analysis was performed using the public domain ImageJ, program developed at the US National Institutes of Health (NIH). It was used to measure the area of pores selected on SEM images. To obtain percent porosity the sum of the areas of the pores was divided by the total exposed sample area.

In liquid displacement method ethanol 100% was used since it can simply infiltrate into the pores without dissolving the polymer. Briefly, the sponge was dipped into a 5 ml graduated cylinder containing a known volume of ethanol (V_1). A series of rapid evacuation– depressurization cycles were assessed to allow the ethanol to penetrate and fill the pores and completely evacuate entrapped air. The volume of ethanol after immersing the scaffold was measured as V_2. The ethanol-impregnated scaffold was taken away from the cylinder and the remaining ethanol volume was recorded as V_3. The porosity of the scaffold was given by the formula
$p = \frac{V_1 - V_3}{V_2 - V_3}$.
In both cases the measures of porosities were the result of a triplicate analysis.

Lactate Dehydrogenase (LDH) Assay

LDH in vitro assay (kit TOX7, Sigma Aldrich) was used to determine cytotoxicity of sponges and microfabricated scaffolds. The enzyme, Lactate DeHydrogenase (LDH), a cytoplasmic enzyme, is a marker for cell membrane integrity. It can be correlated to cell viability since it is released when damage to the cytpolasmic membrane occurs. To perform LDH assay 1·105 cells/cm2 were seeded using a culture medium with reduced serum. Scaffolds were immersed for 72 hours in a phosphate buffered saline (PBS) solution at 37°C with a concentration of 10 mg/ml to assure that any cytotoxic substances were leached (ISO 10993-5:2009 Part 5: Tests for in vitro cytotoxicity).

After incubation, PBS was collected and added to the seeded wells in an amount equal to 1/3 of the medium for 24 hours. LDH in vitro test was carried out following the manufacturer's instructions. Wells seeded with the same concentration of cells and standard culture medium were used as control. The absorbance of the assay mixture was measured at 492 nm ad 600 nm with a photometric microplate reader (Multiskan EX, ThermoLabsystems, Finland). For each type of scaffold four reading of three parallel samples were performed: average value and standard deviation are reported.

Biological characterization

After sterilization with ethanol, 70%, scaffolds were placed in 48-well plates and washed several times with sterile, distilled water. Samples were seeded with 1·104 cells, human osteosarcoma derived osteoblasts (MG63). After 24 hours, scaffolds were moved from the original well plate to a new one to avoid considering cells attached on the tissue culture plate (TCP) and incubated for a total of 28 days. Results were evaluated at five experimental time points: 4, 7, 14, 21 and 28 days. 48-well plates, seeded with the same cell density, were utilized as controls. Minimum essential medium (MEM) supplemented with 10% Fetal Bovine Serum (FBS), 1% Penicillin, 1% Glutamax, 1% Vitamin, 1% non-essential amino acids comprised the culture medium. Cells were incubated at 37ºC in a 5% CO2 atmosphere incubator, with medium changes every 2-3 days.

AlamarBlue Assay

AlamarBlue assay kit (Biosource International Inc., USA) was used to evaluate cell proliferation (proportional to metabolic activity) on 3D scaffolds at the end of each experimental time point. A higher proliferation causes a larger absorbance value as well as a larger percentage of reduced alamarBlue. The assay was performed according to the manufacturer's instructions. In brief, the seeded scaffolds were incubated for 4 hours at 37°C with fresh culture medium (with reduced serum) supplemented with alamarBlue diluted according to manufacturer's data sheet (simply adding the alamarBlue reagent as 10% of the sample volume). A total of three replicates were used for each sample and each replicate was split into four wells for the final reading. The references were taken from wells with unseeded scaffolds incubated with the alamarBlue solution. Absorbance was measured at 570 nm and 600 nm with

a photometric microplate reader (Multiskan EX, ThermoLabsystems, Finland) and the percentage of reduced alamarBlue was calculated [164].

Confocal Laser Microscopy (CLM) imaging

Evaluation of cell attachment, growth, distribution and migration on the seeded scaffolds was performed by confocal laser microscopy (Nikon Eclipse, Ti-E) after Phalloidin Rhodamine (Biosource International, Invitrogen) and DAPI (Sigma Aldrich) staining according to the manufacturer's protocol. Fixation with a formaldehyde solution (4% formaldehyde in PBS solution) and permeabilization with TritonX (0.2% TritonX in PBS solution) were performed before staining.

CLM was also used to evaluate collagen production and distribution after Direct Red 80 (Sigma Aldrich) staining. A published protocol modified specifically for our samples was used [154]. Direct Red 80 staining, more frequently used for collagen detection in tissue histological sections[165, 166, 167], has also been tested to mark collagen for CLM imaging [152]. The staining is not specific for the different types of collagen. Samples were washed in dH20, pre-treated for 40 minutes with a solution of 0.2% phosphomolybdic acid (PMA), and incubated for 30 minutes in a solution consisted of 0.1% Direct Red 80 diluted in saturated aqueous picric acid. At the end each sample was washed in 0.01 M HCl for 2 min. PMA was used to make colorless cytoplasm and HCl was used to remove non specific staining.

Representative images are shown.

Scanning Electron Microscopy (SEM) imaging

Morphological observations were performed with scanning electron microscopy (Supra 40 Zeiss, operating mode: high vacuum, secondary electron detector). Before imaging, biological samples were fixed with a glutaraldehyde solution (2.5% glutaraldehyde in cacodylic buffer solution, 0.1 M) to preserve the structure of living tissues. Then sample dehydration was performed by soaking in a series of aqueous ethanol solutions at increasing concentrations (30% - 50% - 70% - 90% - 100% - 100% v/v) and drying. Before SEM imaging, all samples were sputter coated with gold (SEM Coating Unit PS3, Assing S.p.A., Rome, Italy). Representative images are shown.

Statistical analysis

All values are listed as means with their standard error (mean ± SE). Statistic analyses were performed on the LDH results. F-test of the equality of the variances was conducted with a significance level of 0.05. Unpaired t-test with equal variances was used with a 0.05 significance level.

3.4 Results and Discussion

Collagen behaves as a support structure for tissues, controlling cell shape, differentiation and regeneration. In the intermediate stage of the bone healing process, collagen is the main constituent of callus, which is fundamental because it stabilizes the fracture site, behaves as a support structure for tissue ingrowth and guides the final angiogenesis and tissue mineralization [62]. In particular, the orientation of collagen fibrils leads to the formation of woven, lamellar or primary parallel fibered bone [168]. Soft and hard callus can be considered physiological models for designing biomimetic scaffolds for a tissue engineering approach. A bioresorbable and osteoconductive scaffolding support should trigger and address cell attachment, migration, ECM production, assembling, mineralization and angiogenesis.

In this work the functional role of scaffold geometry as template for physiological callus formation and proper collagen spatial organization was evaluated. After previous scaffold characterization by imaging analyses (SEM) and material cytotoxicity assessment, preliminary biological tests were performed. Cell proliferation, distribution and growth were considered and collagen distribution and arrangement were qualitatively analyzed.

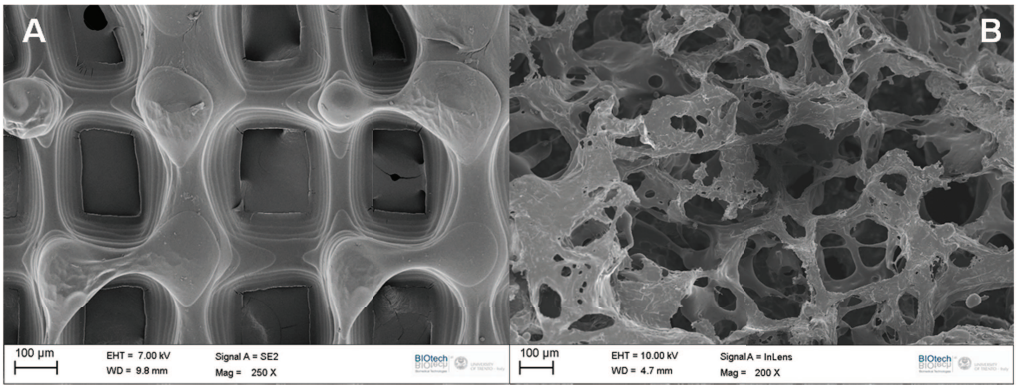

Figure 3.1: Scanning electron microscopy images of PdlLA scaffolds: (A) microfabricated scaffold, (B) salt-leached sponge.

Scaffold morphologies were evaluated by SEM observation and displayed in Fig. 3.1. The results showed that both structures pores were well interconnected but with different shapes, distribution and size ranges. In the salt-leached sponge (Fig. 3.1A), pores were randomly distributed, displaying a biomorphic geometry, with the presence of micro and macro-pores ranging from few microns to about 400 µm. In

contrast, in the microfabricated scaffold (Fig. 3.1B) the pore distribution was quite regular with square shapes, with a side length of around 250 µm. In the microfabricated constructs, the surface appeared smoother and the pore walls appeared thicker than in the salt-leached sponges.

Salt leached sponges porosity was calculated by liquid displacement method and resulted 86% ± 2%. Conversely, microfabricated scaffold porosity, analyzed by ImageJ software, was 61% ± 4%

Cytotoxicity testing on the hypothesis that traces of solvent may have a negative effect on biocompatibility was performed.

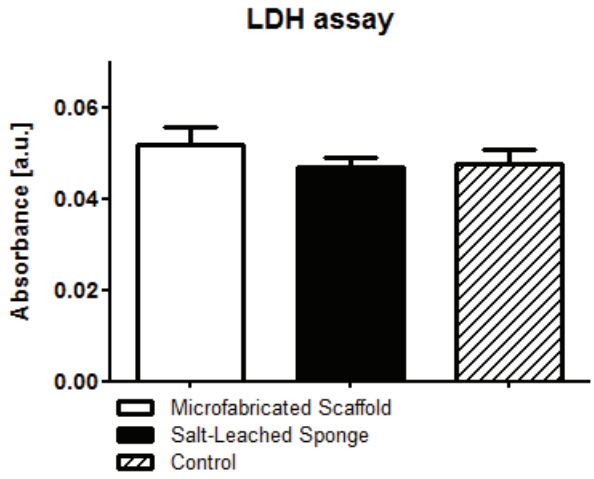

Figure 3.2: LDH assay of PdlLA scaffolds: salt-leached sponges and microfabricated scaffolds are not cytotoxic.

In Fig. 3.2 the average values and standard deviations of the absorbances of the microfabricated scaffolds, salt-leached sponges and control samples are shown. An unpaired t-test with equal variances was used. The means of the absorbance of both the scaffolds compared to the control were the same (with a 0.05 significance level). The cytotoxicity values of scaffolds and control did not appear significantly different.

Preliminary biological evaluations were performed by seeding MG63 cells on salt-leached sponges and microfabricated scaffolds. Seeded samples were incubated for a total of 28 days. Results were evaluated at five experimental time points: 4, 7, 14, 21 and 28 days.

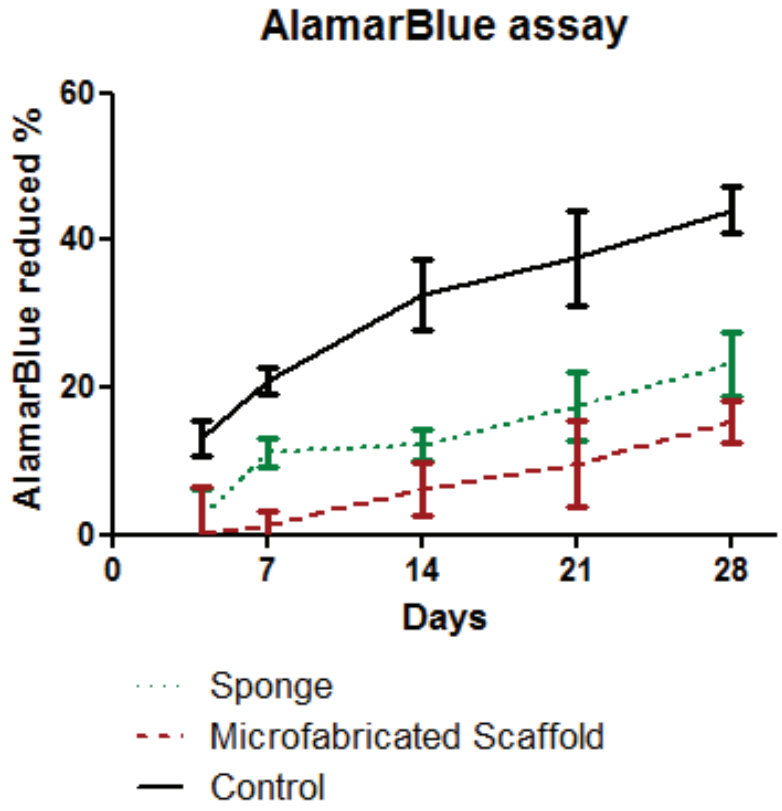

Figure 3.3: AlamarBlue assay for MG63 cell culture on PdlLA scaffolds and 48-well culture plate used as control.

Cell proliferation was assessed using alamarBlue assay. The initial proliferation was substantially higher in the control, tissue culture well plate (TCP), compared to both the scaffold models (Fig. 3.3). The relative absorbance difference of alamarBlue between control samples and scaffolds increased with time. The increase in alamarBlue absorbance with time was higher for salt-leached sponges than for microfabricated scaffolds until day 14, then a similar slope of the curve was shown for the two different matrices and the control. At the last time point, 4 weeks, the values of the alamarBlue assay of seeded salt-leached sponges and microfabricated scaffolds were lower than the control samples. Furthermore, the proliferation of osteoblasts on salt-leached sponges was higher than the proliferation on microfabricated scaffolds.

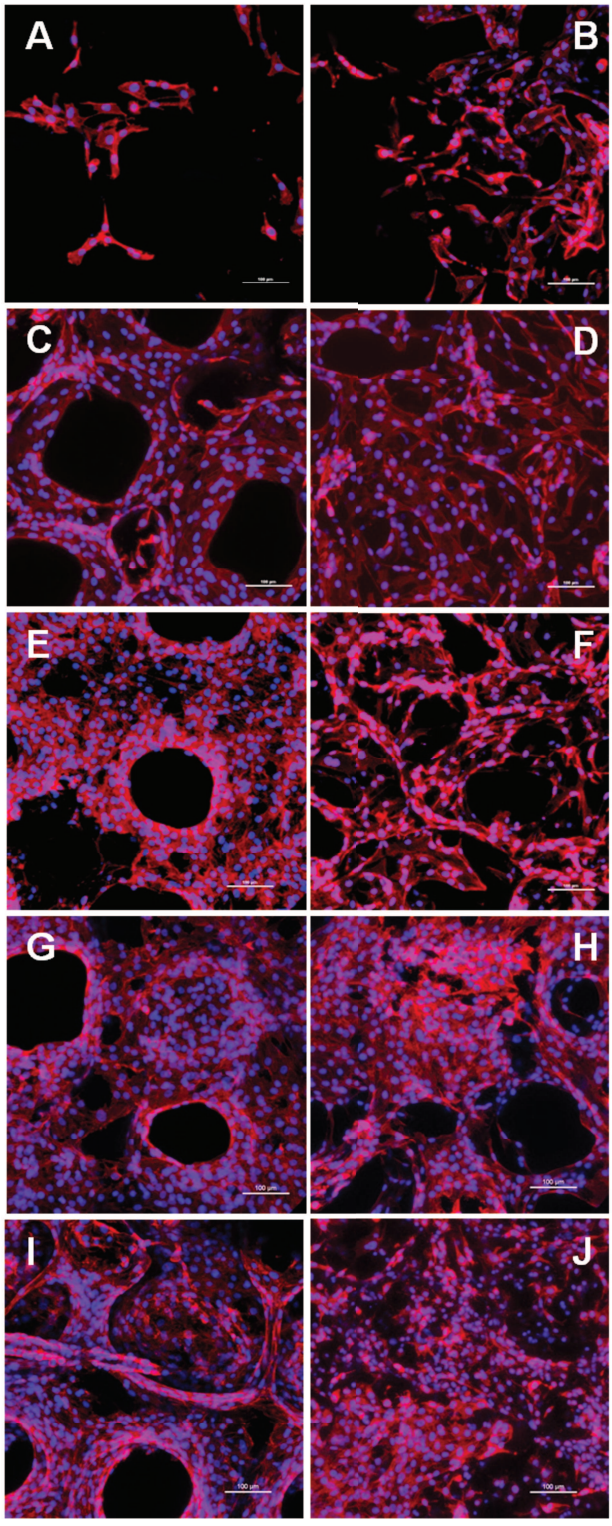

Figure 3.4: Confocal Laser Scanning Microscopy images of MG63 cells stained with Rhodamine Phalloidin and DAPI adhered to PdlLA scaffolds after A, B) 4 days, C, D) 7 days, E, F) 14 days, G, H) 21 days and I, K) 28 days of cell culture. On the left the microfabricated scaffolds, on the right the salt-leached sponges. Scale bars = 100 µm.

The proliferation trend was further confirmed by CLM imaging analyses. Images in Fig. 3.4 show attachment and proliferation of MG63 cells on PdlLA scaffolds. Increase in cell number could be observed with incubation time. Cells started invading scaffold pores and adhering to the matrix. Furthermore, at longer culture time, a deeper migration of cells inside and between the pores was visible. Pore sizes were large enough to permit ingress of cells, with concurrent bridging of cells between pore walls. Fig. 3.4, G and H, show that cells almost completely covered the scaffolds after 21 days of culture.

Cell migration is evident from Fig. 3.5, where confocal depth projection images show the outer and inner part of the seeded scaffolds. The figures result from stacking multiple horizontal images corresponding to different focused planes. The profiling depth is reported on the images.

Microfabricated scaffolds and salt-leached sponges, at the first analyzed time point (Fig. 3.5A and B), showed a cell distribution mainly on the outer surface, where cells were previously seeded. Afterward, the internal regions started to be invaded (Fig. 3.5 C, D, E, F, G, H, I, J). In general, a homogeneous cell distribution was shown within the scaffold thickness indicated.

SEM analyses were in concordance with the confocal microscopy results in terms of cell adhesion and distribution, and also gave a closer view of cell-cell and cell-material interactions.

Cells appear well attached on both constructs but with different adhesion morphology and distribution as shown in Fig. 3.6. Cells seeded on micro-fabricated scaffold adhere to the surface preferably by forming lamellopodia (Fig. 3.6C, white arrow) instead of phyllopodia as in the second model (Fig. 4D, white arrow). But the main difference seems to be their distribution (Fig. 3.6A, B). In the regular geometry, cells seem to prefer to bridge between pore walls, instead to just spread on the surface (Fig. 3.6A, white arrows), so that a new architecture is formed. Interestingly, cells adhered on the salt-leached structure are mainly spread on the surface, so the sponge surface geometry acts as template for cell distribution (Fig. 3.6B, white arrows). The different cell adhesion-distribution can be attributed to the pore distribution and also by the surface roughness. It is also interesting to note that salt-leached sponges, having the more biomorphic geometry similar to bone trabecular structure, may be more readily recognized by bone cells than other configurations.

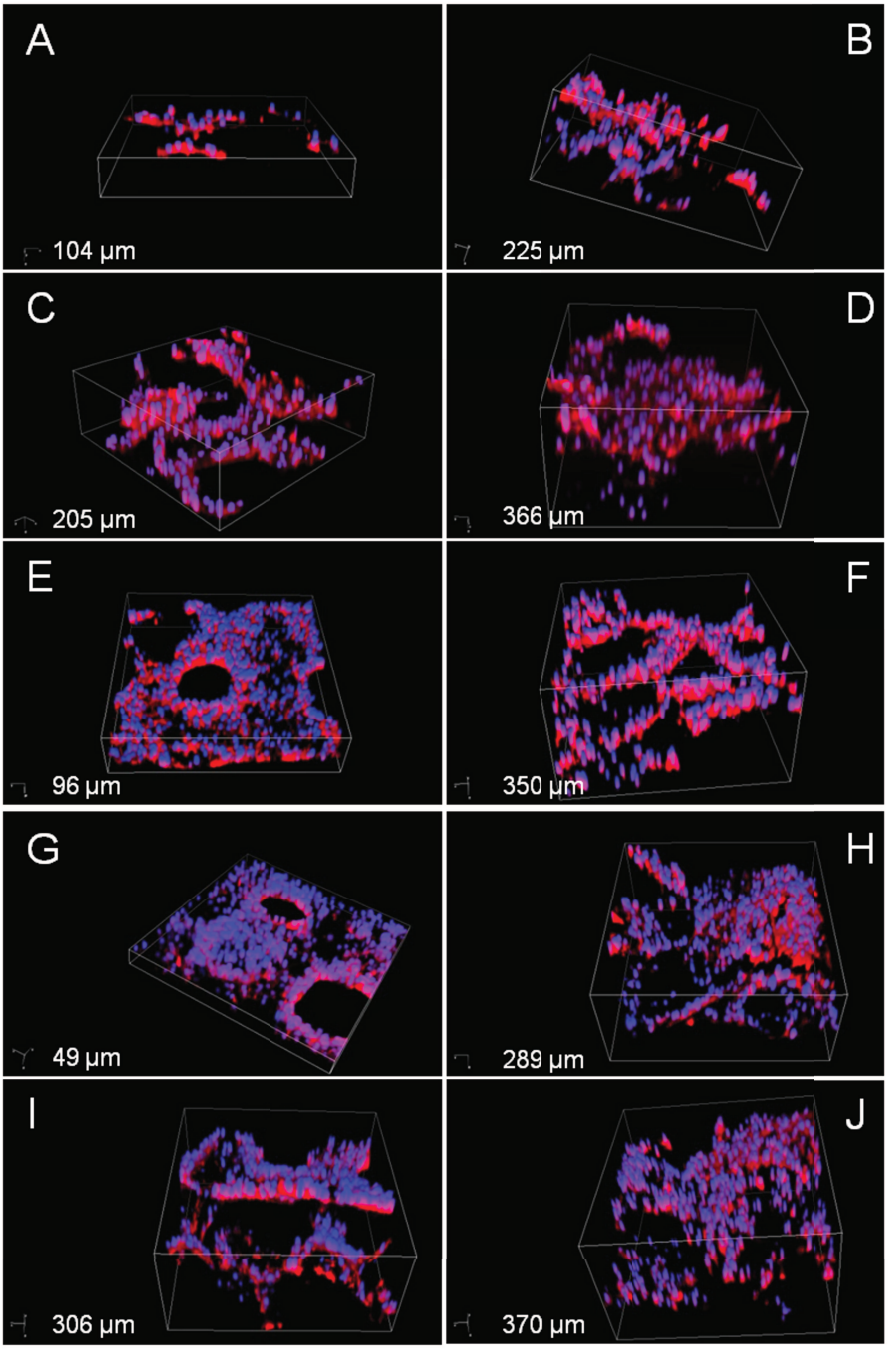

Figure 3.5: 3D Confocal Laser Scanning Microscopy images of MG63 cells stained with Rhodamine Phalloidin and DAPI adhered to PdlLA scaffolds after A, B) 4 days, C, D) 7 days, E, F) 14 days, G, H) 21 days, and J, K) 28 days of cell culture. On the left the microfabricated scaffolds, on the right the salt-leached sponges. Stack depths are specified.

Collagen structure and its network organization, produced by osteoblasts in culture,

was further characterized by a qualitative imaging analyses to check if different scaffold architectures can influence ECM production and assembly. Cells were fixed and stained with Direct Red 80 to visualize the collagen with the confocal microscope.

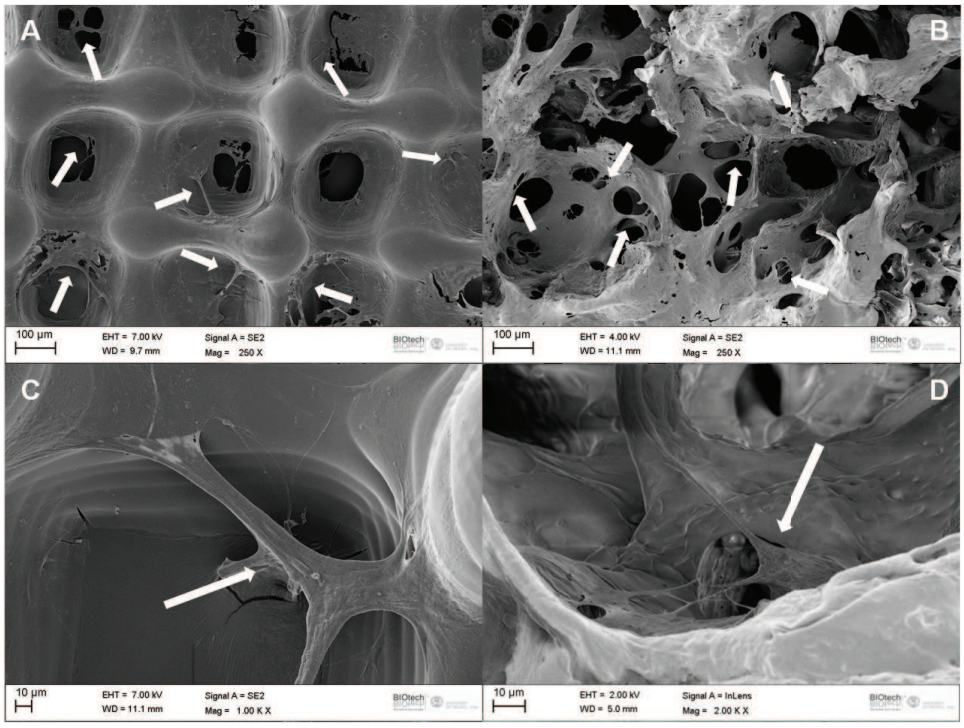

Figure 3.6: SEM images of the PdlLA scaffolds after A, B) 21 days, C, D) 28 days of cell culture. On the left the microfabricated scaffolds, on the right the salt-leached sponges. Arrows indicate cell bridging mechanism and spreading behavior. Different magnification are reported.

CLM images show an increase in collagen amount and a more complex organization with incubation time (Fig. 3.7). Until day 7, collagen structure appeared quite similar on the two different scaffolds: it did not seem organized and the acquired emission signal describes a modest overall amount. Differences were visible at the last cultured time points: in salt-leached sponges a more complex collagen organization could be distinguished. In fact in microfabricated scaffolds (Fig. 3.7J) collagen showed an inhomogeneous planar organization (2D), whereas osteoblasts on salt-leached sponges (Fig. 3.7K) seemed to guide collagen with a fiber-like organized structure arranged more in 3D.

Comparing Fig. 3.4 (I,J) and Fig. 3.7 (I,J) related to the cell and collagen distribution respectively, the effect of scaffold geometry on the collagen assembly process is even more profound than on cell proliferation and distribution.

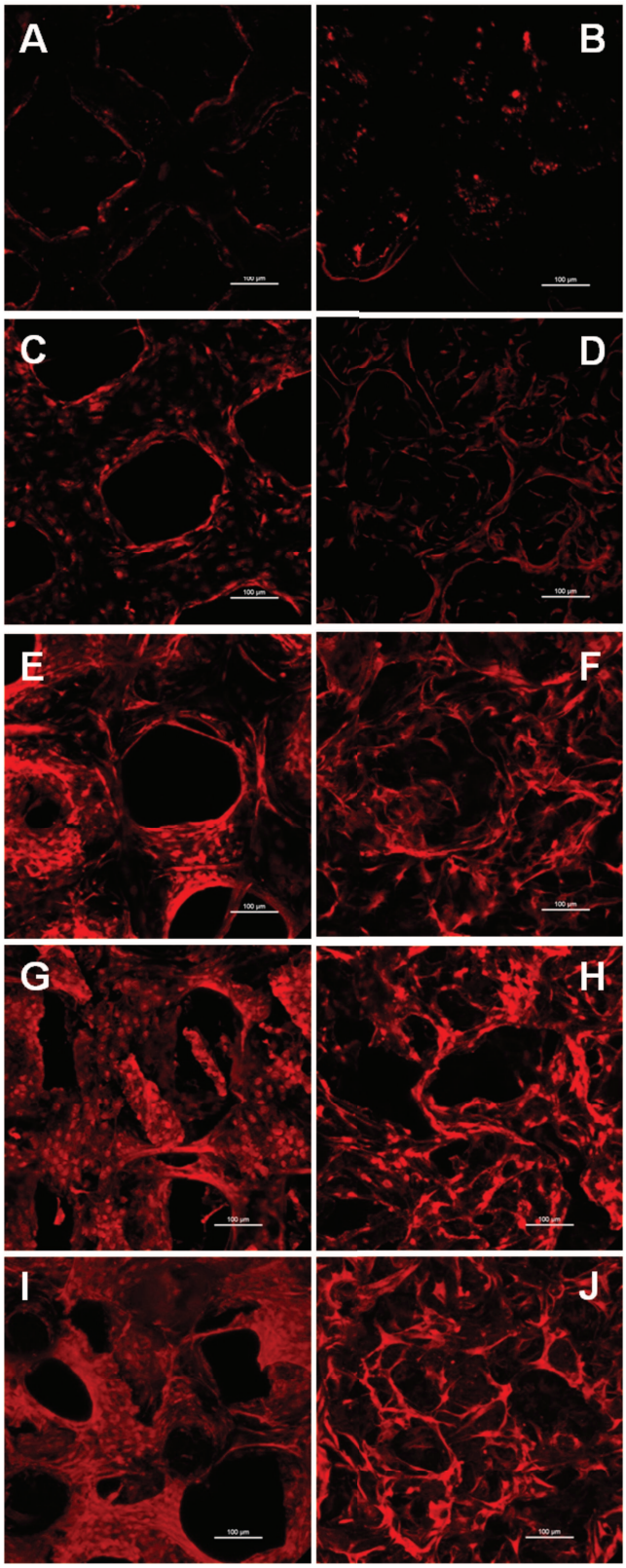

Figure 3.7: Confocal Laser Scanning Microscopy images of MG63 cells stained with Direct Red 80 adhered to PdlLA scaffolds after A, B) 4 days, C, D) 7 days, E, F) 14 days, G, H) 21 days, and J, K) 28 days of cell culture. On the left the microfabricated scaffolds, on the right the salt-leached sponges. Scale bars = 100 µm.

3.5 Conclusions

The functional role of scaffolds with different geometries as templates for physiological collagen mesh formation was studied. Two different 3D porous PdlLA scaffolds provided an appropriate environment for cells growing and good proliferation, as well as effective migration. Furthermore, collagen production and its organization on the scaffolds with a porosity randomly distributed seemed to be more suitable for a bone tissue regeneration application with osteoblasts producing a collagen architecture similar to the natural callus matrix.

The role of soft callus as a template for the final mineralized tissue is fundamental in the bone healing process and, among all the parameters involved, the geometry features of the scaffolds were demonstrated to favorably affect the collagen organization. Further and deeper evaluations to better understand the correlation between scaffold morphology and collagen production and organisation have to be wider elaborated.